25th ABCM International Congress of Mechanical Engineering
October 20-25, 2019, Uberlândia, MG, Brazil

COB-2019-0357
A STRUCTURAL BENCHMARK: AN OPEN CODE APPROACH

Thaynã França
Arthur Braga
Pontifical Catholic University of Rio de Janeiro, R. Marquês de São Vicente, 225 – Gávea, 22451-900
tfranca@id.uff.br abraga@puc-rio.br

Abstract. *The main objective of this work is presents a structural benchmark analysis and also provides an open source implementation. Besides, additional studies, such as: structural parameter variations, different types of damping, systems identification and control can be practiced and valuated on the proposed benchmark. This material brings practicality for both newcomers and experienced users. This code allows structural simulations from a diversified set of excitation signals. The current code based on finite element method with time integration ability is available. In addition, the cited code is made available at https://github.com/tfrancamm/Benchmark-Structure. The proposed three-dimensional structure consists of three rigid bodies connected by twenty-four flexible elements.*

Keywords: *Benchmark, structural dynamics, open code, system identification, variation of parameters.*

1. INTRODUCTION

Notably, the benchmark systems possess a huge relevance in several research fields. An important matter in respect a benchmark system is the capability of improve models, expand the applications and adaptive studies. Thus, this open source code benchmark can be used to realize tasks such as: structural parameter variations, different types of damping, systems identification and control can be practiced and valuated on the proposed benchmark. In the available literature there are other benchmarks. For instance, in (Tiso and Noël, 2017) a benchmark structure based on two offset cantilevered beams connected by a highly flexible element is presented, the authors provide a closed code permitting a restricted numerical simulation of the two-dimensional structure benchmark in respect to arbitrary excitation signals. In order to analyze and control electromechanical oscillations in power system a paper, recommended by the IEEE, condense six benchmark systems obtained from the literature (Canizares et al., 2017).

The paper aims to increase the abundance in respect to robotic view of an inverted pendulum benchmark. Furthermore, the referred paper provides a historical overview and actual trends in relation to nonlinear control theory based on this simple and worthy structure (Boubaker, 2013). A paper presents a surveying of the more relevant developments that appeared in the system identification field since the first six years after the beginning of the second millennium (Noël and Kerschen, 2017). One of these relevant development is about the frequency domain nonlinear subspace identification method. Such method is applied to a numerical benchmark structure (Delli Carri and Ewins, 2014). A control system is applied to a building structure in reduced scale. Such bidimensional structure is discretized by means of the finite element method (Gruzman and Santos, 2016).

In this work the code contains different types of excitation, such as: impulse, harmonic, step and custom force. This custom forcing is given by an input data that contains the forcing of each pavements along the time. In empirical studies, this data can be generated by a sensor. The current code provides the displacements and velocities of each pavement. Besides, a spectral analysis and a spectrogram approaches are depicted as well. Finally, a whole event animation is showed. In this material, all analyses are based on an impulsive excitation. In addition, the number of structural benchmark drastically reduces whether the research is restricted to open source codes. In this study, the structural modelling is treated in three-dimensional form and discretized by means of the finite element method. The next section describes the modeling used in this work. The section 2 handle to the computational implementation also. At last, the section 3 deals with the conclusion.

2. MODELLING AND NUMERIC IMPLEMENTATION

In order to simplify the analysis, in general, continuous systems can be described as systems with several degrees of freedom (Rao, 2008). Thus, the current structure possesses three rigid bodies and twenty-four flexible elements which are identical to each other. The flexible element thickness is considerable smaller than other dimensions of this element. Besides, the first pavement is attached to the ground by means of flexible elements. During whole event each pavement moves parallel to the ground. The Table 1 presents the parameters used in simulation.

Table 1. Simulation parameters.

Property	Parameter
Rigid mass of the first pavement (m_1)	0.500 kg
Rigid mass of the second pavement (m_2)	0.500 kg
Rigid mass of the third pavement (m_3)	0.500 kg
Height of the first pavement (l_1)	0.150 m
Height of the second pavement (l_2)	0.150 m
Height of the third pavement (l_3)	0.150 m
Thickness of the beam (h)	0.001 m
Width of the beam (b)	0.025 m
Elasticity modulus (E)	77 GPa
Specific mass (ρ)	7860 kg m^{-3}
First modal damping factor (ξ_1)	0.007
Second modal damping factor (ξ_2)	0.007
Starting instant of the impulsive disturbance (t_i)	1.00 s
Ending instant of the impulsive disturbance (t_f)	1.01 s
Amplitude of the impulsive disturbance (Λ)	10 N
Frequency of the impulsive disturbance (ω)	314 rad s^{-1}

The cross-sectional area A is represented by Eq. (1).

$$A = hb \tag{1}$$

The Equation (2) denotes the area moment of inertia I.

$$\mathrm{I} = \mathrm{hb}^3/12 \tag{2}$$

The position sensors are added to the system with the purpose of monitoring the pavements displacements. The addressed structure is depicted by Fig. 1. The motion equations obtained by means of the finite element method are given by Eq. (3).

$$\boldsymbol{M\ddot{u}}(t) + \boldsymbol{C\dot{u}}(t) + \boldsymbol{Ku}(t) = \boldsymbol{F}(t) \tag{3}$$

Where $\boldsymbol{M}$, $\boldsymbol{C}$ and $\boldsymbol{K}$ are the mass, Rayleigh damping and stiffness matrices, respectively. Besides, $\boldsymbol{F}(t)$ is the forcing vector applied to the building structure and $\boldsymbol{u}(t)$ is the displacement vector. In its turn, the velocity and acceleration vectors are, respectively, denoted by $\dot{\boldsymbol{u}}(t)$ and $\ddot{\boldsymbol{u}}(t)$.

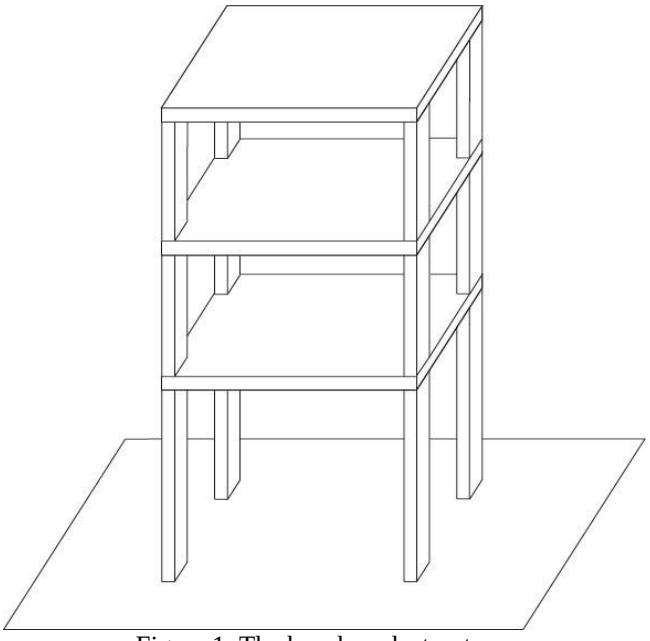

Figure 1. The benchmark structure.

When applying a parallel force to the ground in some of the pavements, the rigid bodies of the structure will remain arranged horizontally throughout event (Falcão, 1977). So, let's assume that the basic element possesses four degrees of freedom, where two are linear and two are rotational $\boldsymbol{u}_1(t)$, $\boldsymbol{u}_2(t)$, $\boldsymbol{u}_3(t)$ and $\boldsymbol{u}_4(t)$, respectively (Inman, 2008). Besides, we admit that the basic element is given by finite, unidimensional and prismatic element. The displacement field $\boldsymbol{u}(x,t)$ provides the transversal displacement. Considering the displacement field represented by a sum of products of a spatial function $\boldsymbol{\psi}(x)$ and a temporal function $\boldsymbol{u}(t)$.

$$\boldsymbol{u}(x,t) \;=\; \sum_{i\,=\,1}^{4} \boldsymbol{\psi}_i(x)\, \boldsymbol{u}_i(t) \tag{4}$$

The spatial functions are called interpolation functions of the basic element. The temporal functions are the nodes displacements of the basic element in relation to the time. Observe that each beam end possesses a node of the basic element. More precisely, the increasing the number of nodes generates more complex interpolation functions. On the other hand, a high number of nodes can imply in a rather realistic model. Since four degrees of freedom are adopted for the basic element, then we can admit third-degree polynomials for the interpolation functions. Note that the Eq. (4) needs four polynomials. These polynomials are given in a dimensionless form by Eq. (5).

$$\boldsymbol{\psi}_i(x) = \; a_i(x/L) + \; b_i(x/L)^2 + c_i(x/L)^3 + \; d_i(x/L)^4 \qquad (i \;=\; 1,\ldots,4) \tag{5}$$

The constants a_i, b_i, c_i and d_i $(i \;=\; 1,\ldots,4)$ are determined by the boundary conditions. Such boundary conditions are given by:

$$\begin{cases} \quad \boldsymbol{u}(0,t) = \; \boldsymbol{u}_1(t) \\ \boldsymbol{\partial u}(0,t)/\boldsymbol{\partial} x \;=\; \boldsymbol{u}_2(t) \\ \quad \boldsymbol{u}(L,t) = \; \boldsymbol{u}_3(t) \\ \boldsymbol{\partial u}(L,t)/\boldsymbol{\partial} x \;=\; \boldsymbol{u}_4(t) \end{cases} \tag{6}$$

In order to obtain the basic element mass matrix, we can approximate the element kinetic energy, described from the time derivatives of the nodes displacements K_C by kinetic energy of the element $K(t)$. This manner, the mass matrix elements are presented by Eq. (7).

$$m_{ij} \;=\; \int_0^L \rho(x)\, A(x)\, \psi_i(x)\, \psi_j(x)\, dx \qquad (i,j \;=\; 1,\ldots,4) \tag{7}$$

If we assume that the specific mass ρ and the elasticity modulus E are constants the basic element mass matrix will be given by:

$$\boldsymbol{\mathcal{M}} \;= (\rho \mathrm{A}/420) \begin{bmatrix} 156\mathrm{L} & 22\mathrm{L}^2 & 54\mathrm{L} & -13\mathrm{L}^2 \\ 22\mathrm{L}^2 & 4\mathrm{L}^3 & 13\mathrm{L}^2 & -3\mathrm{L}^3 \\ 54\mathrm{L} & 13\mathrm{L}^2 & 156\mathrm{L} & -22\mathrm{L}^2 \\ -13\mathrm{L}^2 & -3\mathrm{L}^3 & -22\mathrm{L}^2 & 4\mathrm{L}^3 \end{bmatrix} \tag{8}$$

The basic element stiffness matrix can be approximate using the potential energy of the element, exploited from the nodes displacements U by potential energy of the element $U(t)$.

$$k_{ij} \;=\; \int_0^L E(x)\, I(x)\, \psi_i(x)\, \psi_j(x)\, dx \qquad (i,j \;=\; 1,\ldots,4) \tag{9}$$

Since the geometric properties of the elements are constants hence, the area moment of inertia will also be. Thus, we conclude that the stiffness matrix of the flexible beam element is depicted by:

$$\boldsymbol{\mathcal{K}} \;= (\mathrm{EI}/\mathrm{L}^3) \begin{bmatrix} 12 & 6\mathrm{L} & -12 & 6\mathrm{L} \\ 6\mathrm{L} & 4\mathrm{L}^2 & -6\mathrm{L} & 2\mathrm{L}^2 \\ -12 & -6\mathrm{L} & 12 & -6\mathrm{L} \\ 6\mathrm{L} & 2\mathrm{L}^2 & -6\mathrm{L} & 4\mathrm{L}^2 \end{bmatrix} \tag{10}$$

The Figure 2 indicate the basic element adopted with the purpose to discretize the structure as a whole and the nodes obtained by the finite element method. Let`s admit twenty-four beams in the whole structure, where we have eight beams in each pavement. This way, we have a total of twenty-seven degrees of freedom. The local displacements fields $\boldsymbol{u}_i$ $(i = 1, \ldots, 24)$, the global displacement field $\boldsymbol{u}$ and the transformation matrices $\boldsymbol{T}_i$ $(i = 1, \ldots, 24)$.

$$\boldsymbol{u}_i = \; \boldsymbol{T}_i \boldsymbol{u} \quad (i = 1, \ldots, 24) \tag{11}$$

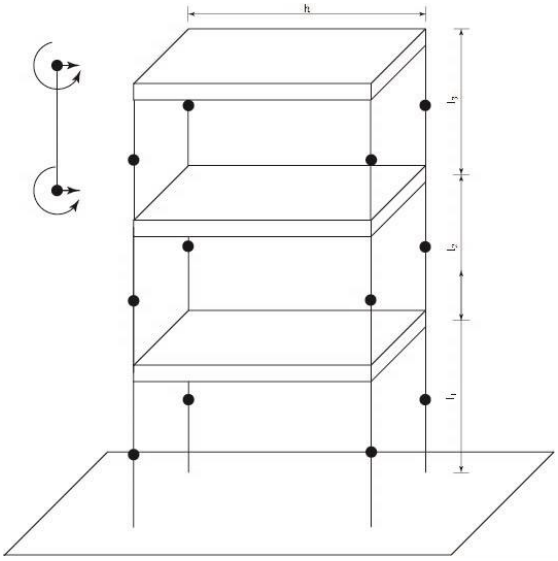

Figure 2. The nodes arrangement and basic element adopted.

The rigid mass matrix $\bar{\boldsymbol{M}}$, i.e., the mass matrix which take into consideration the influence of the horizontal rigid bodies are presented by:

$$\bar{\boldsymbol{M}} = \bar{m}_{ij} = \begin{cases} m_1 & ; i = j = 9 \\ m_2 & ; i = j = 18 \\ m_3 & ; i = j = 27 \\ 0 & ; \text{elsewhere} \end{cases} \tag{12}$$

The global mass matrix $\boldsymbol{M}$ are showed in Eq. (13). In addition, the degrees of freedom u_9, u_{18} and u_{27} represents, respectively, the displacements of the first, second and third pavements.

$$\boldsymbol{M} = \sum_{I=1}^{24} [(\boldsymbol{T}_i)^{\mathrm{T}} \boldsymbol{\mathcal{M}}_{\mathrm{i}} \boldsymbol{T}_i] + \bar{\boldsymbol{M}} \tag{13}$$

At last, the global stiffness matrix $\boldsymbol{K}$ is denoted by:

$$\boldsymbol{K} = \sum_{I=1}^{24} [(\boldsymbol{T}_i)^{\mathrm{T}} \boldsymbol{\mathcal{K}}_{\mathrm{i}} \boldsymbol{T}_i] \tag{14}$$

The critical frequencies belonging to a set of zero to five hundred hertz are showed in Tab. 2. The critical frequencies of the structure are calculated by Eq. (15).

$$|\boldsymbol{K} - \omega_n^2 \boldsymbol{M}| = 0 \tag{15}$$

The first modal damping factor ξ_1 and the second modal damping factor ξ_2 can be extracted from the literature or from experiments (Inman, 2008).

$$\begin{cases} \xi_1 = \alpha/(2\omega_1) + (\beta\omega_1)/2 \\ \xi_2 = \alpha/(2\omega_2) + (\beta\omega_2)/2 \end{cases} \tag{16}$$

The global damping matrix $\boldsymbol{C}$ is presented by means of the Rayleigh damping, where the coefficients α and β are given by the Eq. (16).

$$\boldsymbol{C} = \alpha\boldsymbol{M} + \beta\boldsymbol{K} \tag{17}$$

The solution of Eq. (15) are related with the natural frequencies of the undamped system ω_n. External excitations close to the natural frequencies can induce catastrophic failure. The impulsive force parallel to the ground applied to the highest level of the structure are given by:

$$\boldsymbol{f}_{\mathbf{I}}(t) = \begin{cases} 0 & ; t < t_i \\ \Lambda \sin(\omega t) & ; t_i < t < t_f \\ 0 & ; t > t_f \end{cases} \tag{18}$$

Table 2. Critical frequencies in the $0 - 500$ Hz frequency range.

Mode	Critical frequency [Hz]
1	4.4
2	12.5
3	18.3
4	145.3
5	145.8
6	149.4
7	153.8

The current computational implementation is based on the fourth-order Runge-Kutta method with fixed step size. Let's assume that the structure is subjected to small oscillations. So, after the force application $\boldsymbol{F}(t)$ the rigid bodies of the structure will move parallel to the ground.

$$\boldsymbol{F}(t) = \boldsymbol{F}_i(t) = \begin{cases} 0 & ; i = 1, \dots, 26 \\ \boldsymbol{f_1}(t) & ; \ i = 27 \end{cases} \tag{19}$$

The nodes displacements are presented by:

$$\boldsymbol{u}(t) = \{u_1(t) \ \ u_2(t) \ \dots \ u_{27}(t)\}^{\mathrm{T}} \tag{20}$$

In order to obtain the numerical solution of the ordinary differential equation system, it is necessary to make a replacement variable. Thus, based on this replacement variable approach, we will acquire a first-order ordinary differential equation system.

$$\dot{\boldsymbol{u}}(t) = \boldsymbol{v}(t) \tag{21}$$

At last, the referred system is represented by:

$$\begin{cases} \boldsymbol{M}\dot{\boldsymbol{v}}(t) + \boldsymbol{C}\boldsymbol{v}(t) + \boldsymbol{K}\boldsymbol{u}(t) = \boldsymbol{F}(t) \\ \dot{\boldsymbol{u}}(t) = \boldsymbol{v}(t) \end{cases} \tag{22}$$

The Figure 3 shows the three pavements displacements about a quarter of minute given by the finite element method.

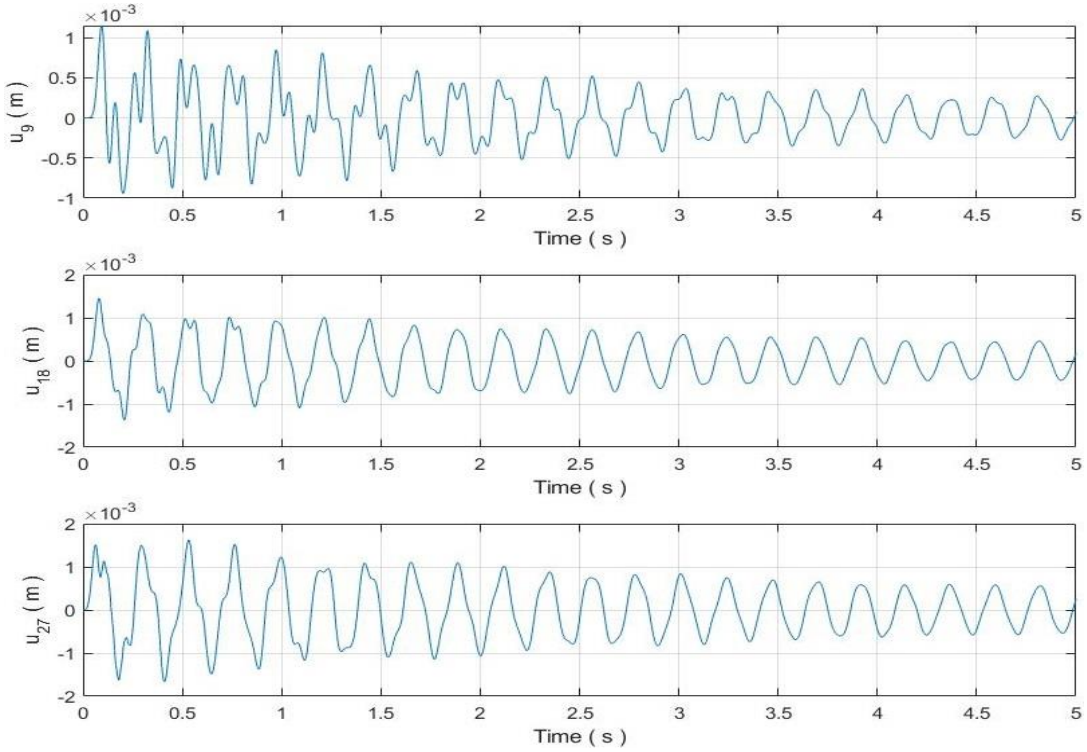

Figure 3. Displacement in respect to each pavement.

The spectrographic analysis possesses one hundred segments partitioning the siginal with ninety-nine overlapped samples. Into the bargain, one hundred sampling points are used as a parameters of the discrete Fourier transform. This way, a good resolution is expected. The Figure 4 depict the spectrograms related to the displacements when the cited impulse is applied. Thus, it is possible to observe that there are three frequencies are remarkable in the spectrographic study.

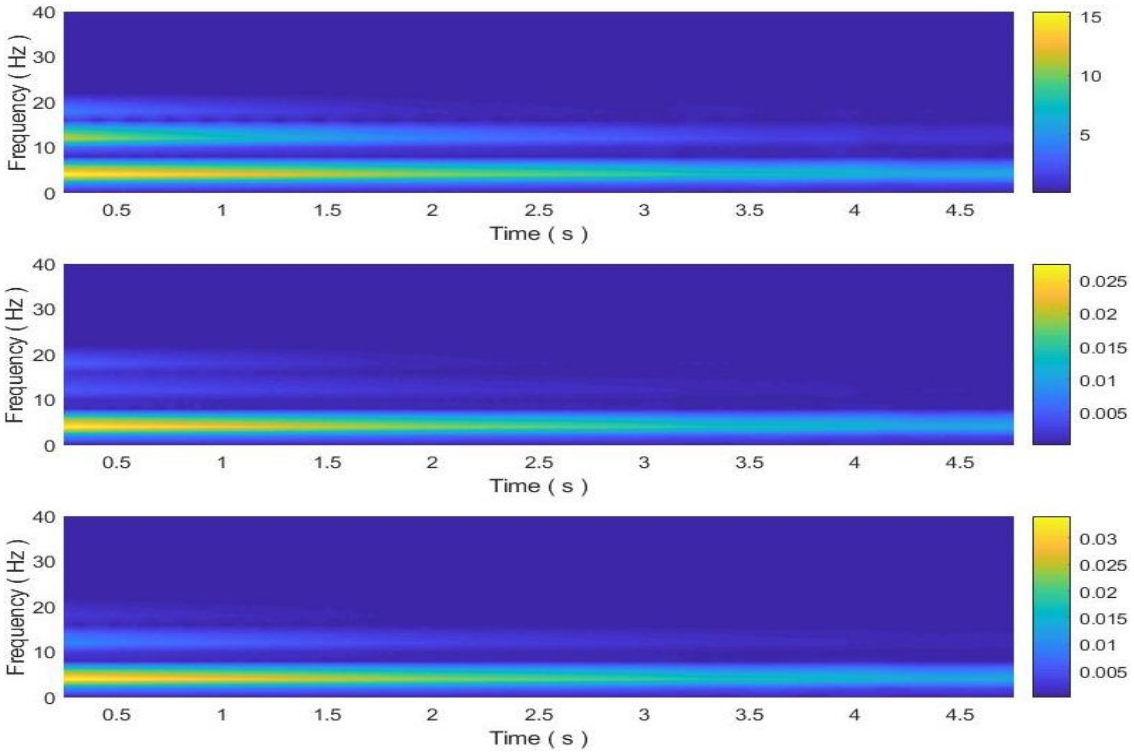

Figure 4. The spectrograms related to the pavements displacements.

The Figure 5 exploit the three pavements displacements in frequency domain. The frequency domain approach is given by using the logarithmic scale on both the horizontal and vertical axes. In the previous referred approach, it is also possible to perceive that there are three notable frequencies. Both in the spectrographic analysis and in the frequency domain analysis it can be observed that such dominant frequencies are in the range of zero to twenty hertz.

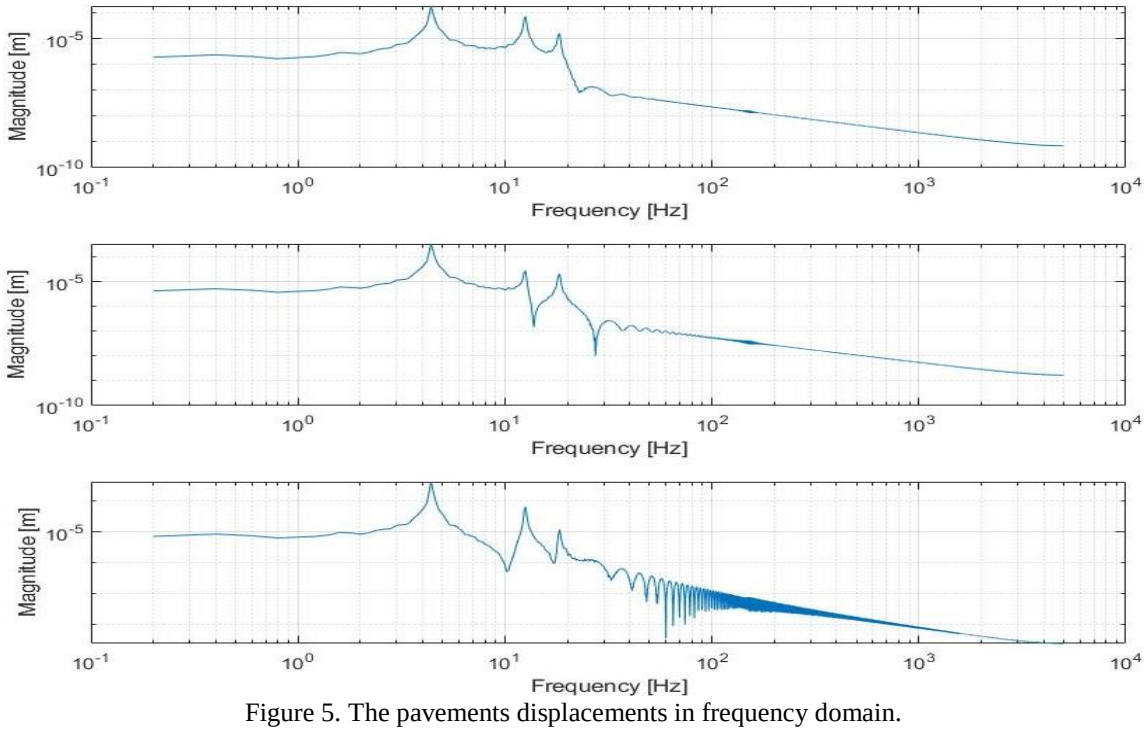

Figure 5. The pavements displacements in frequency domain.

Other two distinct types of structural load can be represented by real physical problems. These families exploit conditions, respectively, depicted by an unbalanced rotational motor and a wind load, for instance. Thus, let's assume that the first one is given by a harmonic force with the same amplitude of the impulsive load and the frequency is represented by the first critical frequency ω_1. The Eq. (23) describes the applied harmonic excitation.

$$\boldsymbol{f_H}(t) = \Lambda \sin(\omega_1 t) \tag{23}$$

The second one are defined by a ramp excitation, where the maximum ramp force is also given by the amplitude of the impulsive load. Besides, this maximum value is reached in a time percentage η with respect to the total time of simulation t_t. This manner, the ramp load is represented by:

$$\boldsymbol{f_R}(t) = \begin{cases} \Lambda t/\eta & ; \ 0 < t < \eta \\ \Lambda & ; \ \eta < t < t_t \end{cases} \tag{24}$$

In both last excitation cases, the total time of simulation is ten seconds. Notwithstanding, the time percentage is thirty percent in relation to the total time of simulation. The previous cited excitations are applied in the highest floor of the structure. Since the harmonic excitation frequency is near to the first critical frequency of the system, are expected large displacements. Thus, it is possible to observe the high amplitude reached because of the frequency adopted. The pavements displacements, in each case, are described by the Figure 6. The supplied code by this material is capable of providing the velocity and acceleration of each floor. In addition, the spectral analysis and the spectrogram approach can be obtained by means of the same code. In order to enrich this study, the cited open code also provides an animation of the structure behavior based on the applied excitation. The referred animation is exaggerated to ensure the structure behavior is more visible.

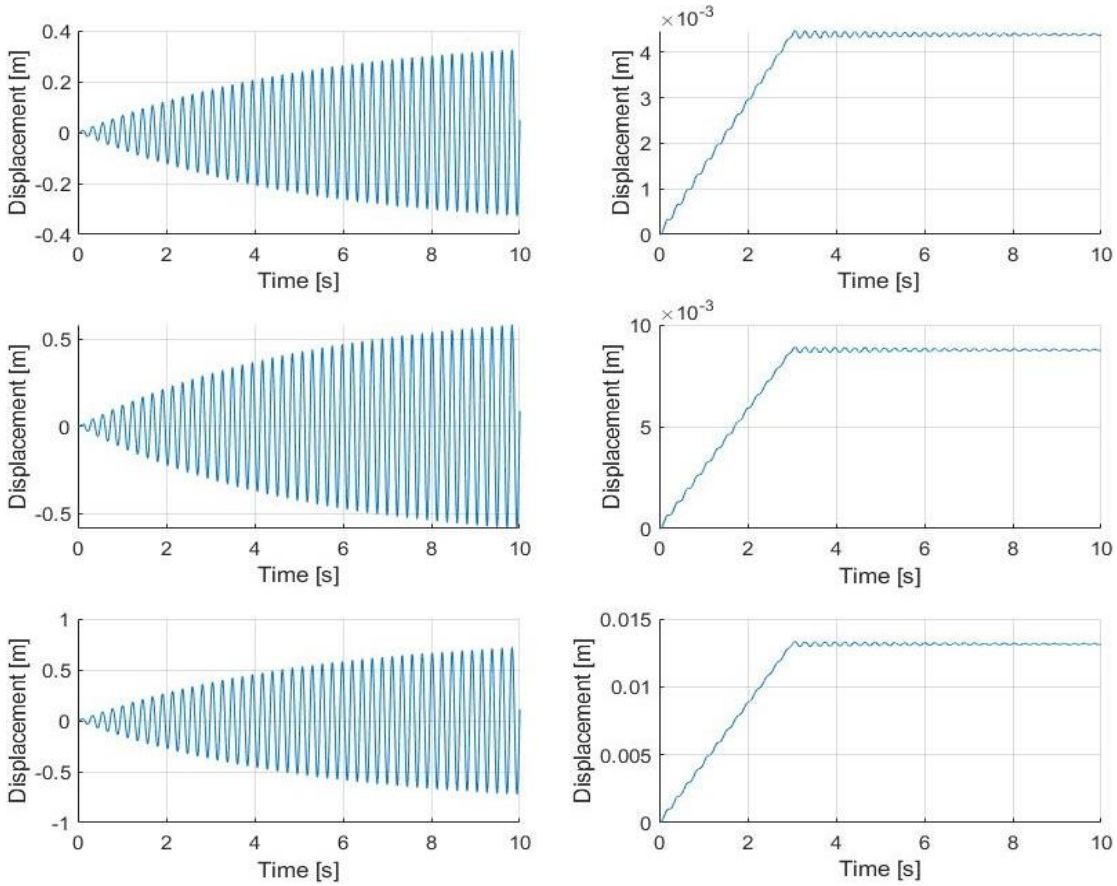

Figure 6. The displacements obtained by means of a harmonic excitation (left) and a ramp excitation (right).

3. CONCLUSIONS

This code can be useful in different levels of application. In a computational and an engineering point of view, the open source code provides the understanding of each process part, as well as all the process. In addition, this code makes feasible to compare with other similar structure modeling or a physics structure. At last, the current code can be applied as a starting point for system identification or control implementation.

4. ACKNOWLEDGEMENTS

The first author of this paper would like to thank Coordenação de Aperfeiçoamento de Pessoal de Nível Superior (CAPES) of Brazil and the Fundação de Amparo à Pesquisa do Estado do Rio de Janeiro (FAPERJ) of Brasil for their financial supports – Finance Code 001.

5. REFERENCES

Boubaker, O., 2012. "The inverted pendulum benchmark in nonlinear control theory: A survey". *International Journal of Advanced Robotic Systems*, Vol. 10, No. 5.

Canizares, C., Fernandes, T., Geraldi, E., Gerin-Lajoie, L., Gibbard, M., Hiskens, I., Kersulis, J., Kuiava, R., Lima, L., DeMarco, F., Martins, N., Pal, B.C., Piardi, A., Ramos, R., Santos, J., Silva, D., Singh, A.K., Tamimi, B. and Vowels, D., 2017. "Benchmark Models for the Analysis and Control of Small-Signal Oscillatory Dynamics in Power Systems". *IEEE Transactions on Power Systems*, Vol. 32, No. 1, pp. 715–722.

Delli Carri, A. and Ewins, D.J., 2014. "Nonlinear identification of a numerical benchmark structure: from measurements to FE model updating". In *Proceedings of the 26th International Conference on Noise and Vibration Engineering - ISMA 2014 and 5th International Conference on Uncertainty in Structural Dynamics – USD 2014*. Leuven, Belgium.

Falcão, M.D., 1977. "Análise Matricial das Estruturas". Livros Técnicos e Científicos.

Gruzman, M. and Santos, I.F., 2016. "Vibration control of a flexible structure with electromagnetic actuators". *Journal of the Brazilian Society of Mechanical Sciences and Engineering*, Vol. 38, No. 4, pp. 1131–1142.

Inman, D.J., 2008. "Engineering Vibration". *Pearson Education International*.

Noël, J.P. and Kerschen, G., 2017. "Nonlinear system identification in structural dynamics: 10 more years of progress". *Mechanical Systems and Signal Processing*, Vol. 83, pp. 2–35.

Rao, S.S., 2008. "Vibrações Mecânicas". *Pearson Education International*.

Tiso, P. and Noël, J.P., 2017. "A new, challenging benchmark for nonlinear system identification". *Mechanical Systems and Signal Processing*, Vol. 84, pp. 185–193.

6. RESPONSIBILITY NOTICE

The authors are the only responsible for the printed material included in this paper.